Jump at the Onset of Saltation

M. V. Carneiro,[1] T. Pähtz,[1] and H. J. Herrmann[1,2]

[1]*Institut für Baustoffe, ETH-Hönggerberg, Schafmattstrasse 6, 8093 Zürich, Switzerland*
[2]*Departamento de Física, Universidade Federal do Ceará, 60451-970 Fortaleza, Ceará, Brazil*

(Received 14 April 2011; published 26 August 2011)

We reveal that the transition in the saturated flux for aeolian saltation is generically discontinuous by explicitly simulating particle motion in turbulent flow. This is the first time that a jump in the saturated flux has been observed. The discontinuity is followed by a coexistence interval with two metastable solutions. The modification of the wind profile due to momentum exchange exhibits a maximum at high shear strength.

DOI: 10.1103/PhysRevLett.107.098001 PACS numbers: 45.70.Mg, 47.27.−i, 47.55.Kf, 83.80.Hj

Aeolian saltation is one of the main actors of molding Earth's landscape. It not only has impact on the evolution of the agricultural areas but also on the change of river courses and the motion of sand dunes. Saltation consists in the transport of sand or gravel by air or water and occurs when sand grains are lifted and accelerated by the fluid, hopping over the surface and ejecting other particles [1,2]. The proper measurement of saltation close to the impact threshold through experiments is strongly limited by technical difficulties. Because of temporal fluctuations, one obtains unreliable data and large error bars. The computational simulation of aeolian saltation, however, can monitor every mechanical interaction between particles giving local insight about the particle splash and, in particular, about the system close to the impact threshold. Here, we report for the first time the existence of a discontinuity in the flux at the onset of saltation using discrete elements.

Saltation was first described by Bagnold's seminal work discussing the particle splash and proposing a cubic relation between wind shear velocity and saturated mass flux [3–5]. Greeley *et al.* [6] confirmed experimentally Bagnold's result and Ungar and Haff [7] complemented it in their numerical model with a quadratic relation near the impact threshold. Anderson and Haff [8,9] studied numerically the statistical properties of the particle splash relating the number and velocities of ejected particles to the impacting ones. Splash entrainment was carefully studied in experiments [10–13] and used in nonsteady saltation models [14,15] finding that the splash mechanism dominates the saturation of sand flux. Recently, Almeida *et al.* [16,17] implemented the full feedback with the fluid and fixed splash angle while Kok and Renno [18] used a splash entrainment function, both resulting in good agreement with experiments. These and other theoretical studies, e.g., [19–21], however, describe the sand bed as a rough wall instead of resolving it at the particle scale and consequently rely on an empirical splash function.

We present a discrete element simulation for aeolian saltation which does not require the use of a splash function. Particles are subjected to gravity g and dragged by a height-dependent wind field. The unperturbed wind profile is [2]

$$u(y) = \frac{u_*}{\kappa} \ln \frac{y - h_0 + y_0}{y_0}, \tag{1}$$

where y_0 is the roughness of the bed, u_* the wind shear velocity, $\kappa = 0.4$ the von Kármán constant, and h_0 the bed height, below which the wind velocity is zero. We adopted the widely used roughness law, $y_0 = D_{\mathrm{mean}}/30$, measured by Refs. [22,23] for hydrodynamically rough pipe flow and confirmed by Ref. [5] for air flow, where D_{mean} is the mean diameter of the particles. A particle of diameter D is accelerated by the wind drag force given by [2]

$$F_d = -\frac{\pi D^2}{8} \rho_a C_d v_r \mathbf{v_r}, \tag{2}$$

where ρ_a is the air density and $\mathbf{v_r} = \mathbf{v} - \mathbf{u}$ is the velocity difference between particle and air, with $v_r = |\mathbf{v_r}|$. The drag coefficient C_d proposed by Cheng [24] is suited to model natural and irregularly shaped grains:

$$C_d = \left[\left(\frac{32}{\mathrm{Re}}\right)^{2/3} + 1\right]^{3/2}, \qquad \mathrm{Re} = \frac{\rho_a v_r D_{\mathrm{mean}}}{\mu}, \tag{3}$$

where $\mu = 1.8702 \times 10^{-5}$ kg/(m · s) is the dynamic viscosity and Re is the Reynolds number, which together with the Shields number θ below are the pertinent dimensionless parameters of our problem:

$$\theta = \frac{u_*^2}{(s-1) g D_{\mathrm{mean}}}, \tag{4}$$

where $s = \rho_s/\rho_w$ is the ratio between the grain and fluid density.

The detailed integration of the wind profile considering the momentum exchange is explained in the Supplemental Material [25].

An aerodynamic lift arises from shear in the flow, which results in a pressure gradient normal to the shear in the direction of decreasing velocity. This aerodynamic lift can be approximately described by [2]

$$F_l = \frac{\pi D^3}{8} \rho_a C_l \nabla v_r^2, \tag{5}$$

where the lift coefficient C_l is proportional to C_d [26].

The vertical motion of the particle is given by the competition between the gravity g, lift forces, and the rebouncing of particles with the ground.

Alternatively, instead of lift forces, we also did some simulations perturbating the system at rest by lifting up at every real second a fraction $c = 0.2$ of the surface particles by a height D_{mean} in order to restart the saltation.

We considered a disordered bed with 500 spherical particles initially at rest in a two-dimensional system (see Fig. 1). The diameters are randomly chosen from a Gaussian distribution around D_{mean} of width $0.15 D_{\text{mean}}$. We simulated systems with more particles to verify that the bottom wall effects are negligible as discussed in Refs. [10,11]. Within the error bars, they displayed identical properties and therefore we did not need to consider larger systems. At $t = 0$, some particles are dropped from randomly chosen heights and when they reach the ground they collide with particles at rest inside the bed and thereby trigger saltation. The particle collisions are computed using the discrete elements method.

Trajectories are obtained by integrating the equations of motion according to the velocity-Störmer-Verlet scheme [27], using a spring dashpot potential with the spring constant k and a dissipative damping parameter γ. Further details about the technique are explained in the Supplemental Material [25]. The dissipative rate of the lower boundary was set high enough, $\gamma_w = 0.8$, to avoid the ejection of additional particles. This can be caused when a shock wave generated by an impacting particle is reflected at the bottom wall [11].

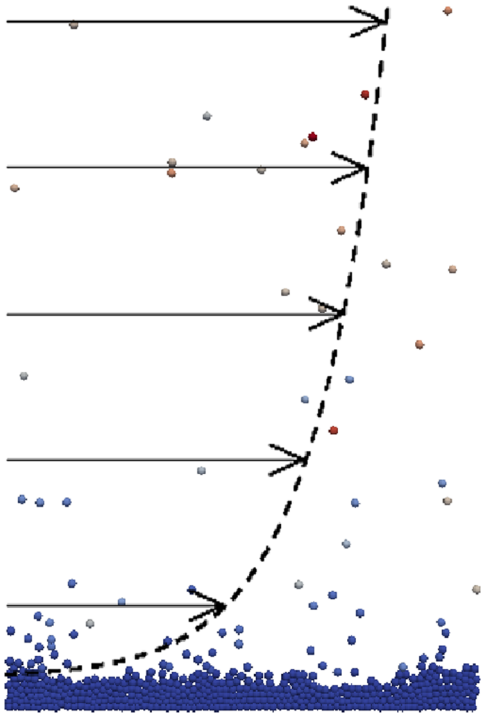

FIG. 1 (color online). Snapshot of the simulation with an initially logarithmic wind profile. Colors represent the particle velocity.

Space is sliced in vertical rectangular domains of size $(250 \times 75) D_{\text{mean}}$. The top is placed sufficiently high to mimic an open system. Periodic boundary conditions are imposed in wind direction and top and bottom boundaries are reflective.

We measure the particle flux through

$$q = \frac{1}{A} \sum_i^N m_i v_i^x, \tag{6}$$

where v_i^x is the particle velocity in the x direction. The saturated flux is the average flux in the stationary state. Simulated systems with different number of particles display similar flux. The dimensionless flux can be obtained by

$$\tilde{q} = \frac{q}{\rho_s \sqrt{(s-1) g D_{\text{mean}}^3}}, \tag{7}$$

where ρ_s is the grain density.

We verified numerically that the dimensionless saturated flux remains invariant under changes of the parameters as long as the Reynolds number and Shields number are fixed.

Simulations verify the existence of an onset velocity for sustained flux $\theta_c = 0.048$ with strong temporal fluctuations as illustrated in Fig. 2. Below this value the flux will stop after some time. This happens because an impact may not necessarily eject other particles that can carry on saltation, and once the flux is zero it cannot restart unless a perturbation or lift force is introduced.

In Fig. 2(a) below the onset, the system fell at rest during the 8th second. So some perturbations were introduced at $t = 9$, 10, and 11 s in order to trigger saltation, after it

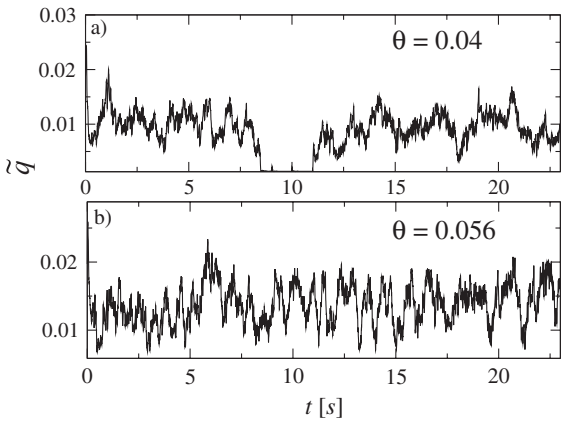

FIG. 2. Flux series for two different Shields numbers near the onset. In (a), the system was perturbed at $t = 9$, 10, and 11 s to keep the flux different from zero, while in (b) the system never settled down.

stopped. Only, the perturbation at $t = 11$ s was able to restart the saltation and the flux returned to the previous levels.

We denote by θ_t the Shields number below which the previously defined perturbations or lift forces according to Eq. (5) are not sufficient to restart saltation and by θ_c the critical Shields number above which the perturbations are no longer needed to maintain saltation. For $\theta_t < \theta < \theta_c$, the system displays a metastable behavior with two possible solutions, either saltation or no motion, strongly dependent on the initial conditions and the triggering mechanism. In our model, we obtained $\theta_t \simeq 0.038$ for perturbations with $c = 0.2$ and $\theta_c = 0.048$. The fact that perturbations are necessary to sustain saltation underlines the importance of the turbulent lift forces in the metastable region.

Figure 3(a) presents the saturated flux for different Shields numbers in comparison with field and wind tunnel experimental data from Iversen and Rasmussen [28]. The calculated data are well fitted using $\tilde{q}_s = \tilde{q}_0 + A(\theta - \theta_c)\theta^{1/2}$ with $A = 1.52$ and $\tilde{q}_0 = 0.01$, which is similar to the relation proposed in Ref. [29]. Figure 3(b) presents details of the discontinuous transition at θ_c with a jump $\tilde{q}_0$ in the saturated flux. The triangles are the data including perturbations and the squares are the data with lift forces. Additional simulations show that θ_t and the jump $\tilde{q}_0$ depend on the lift coefficient C_l.

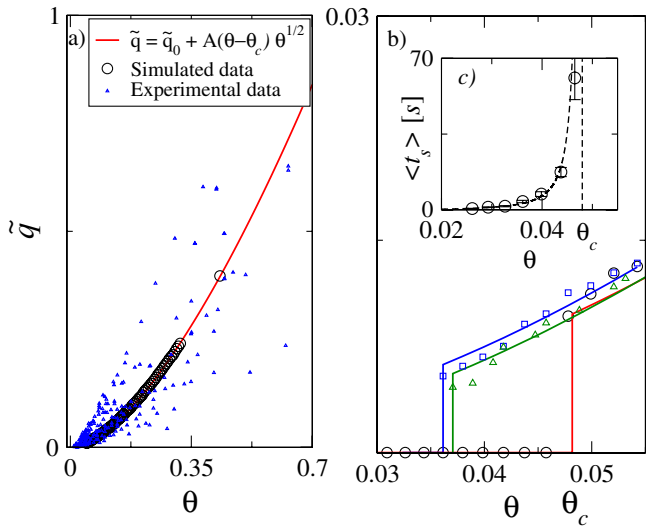

FIG. 3 (color online). Saturated flux as function of the Shields number. (a) Simulated data fitted by $\tilde{q}_s = \tilde{q}_0 + A(\theta - \theta_c)\theta^{1/2}$, $\tilde{q}_0 = 0.01$, $A = 1.52$, and $\theta_c = 0.048$ in comparison with experimental data [28]. (b) Detailed view of the metastable region of the discontinuous transition. The green curve with triangles and the blue curve with squares are the results including perturbations with $c = 0.2$ and lift forces with $C_l = 0.425C_d$, respectively. (c) Average transient time to settle without perturbation in the metastable region. The dashed line fits the time distribution according to $t_s = t_0[\theta/(\theta_c - \theta)]^p$ with $t_0 = 0.524$ s, $p = 1.5$, $\theta_c = 0.048$.

Figure 3(c) presents the average transient time $\langle t_s \rangle$ it takes for the system to settle without perturbation or lift diverging when $\theta \to \theta_c$. The dashed line fits the data according to $t_s = t_0[\theta/(\theta_c - \theta)]^p$ with $t_0 = 0.052$ s, $p = 1.5$. The transient times $\langle t_s \rangle$ were averaged over 60 simulations with different initial conditions.

The discontinuity in the saturated flux is verified also at the same value θ_c using the drag coefficient from Ref. [30] and is shifted in the velocity axis by the dissipation rate γ, i.e., to lower (higher) critical velocities for lower (higher) dissipation rates. Interestingly, we were able to find the same discontinuous transition and metastable region also using the code of Ref [18].

Figure 4 shows the momentum transfer to the particles as a function of height for different Shields numbers. Because of the higher concentration of particles, the largest momentum transfer occurs close to the bed surface. Additionally, this region coincides with the one in which we observe small changes in the modified wind profile in Fig. 1 in the Supplemental Material [25]. Momentum transfer for high Shields number exhibits a local maximum, which gets more pronounced with increasing the Shields number. As shown in Fig. 4(b), high Shields numbers enhance the concentration at higher y where the wind profile grows stronger. This increases momentum transfer at this level. In Fig. 4(b), we see that in fact the concentration exhibits a saddle point at the same height at which the maximum in momentum transfer appears.

Figure 5 shows modified velocity profiles for $\theta > \theta_c$ crossing each other at a focal point, called the "Bagnold focus" [5] and approximately located 0.5 cm above the

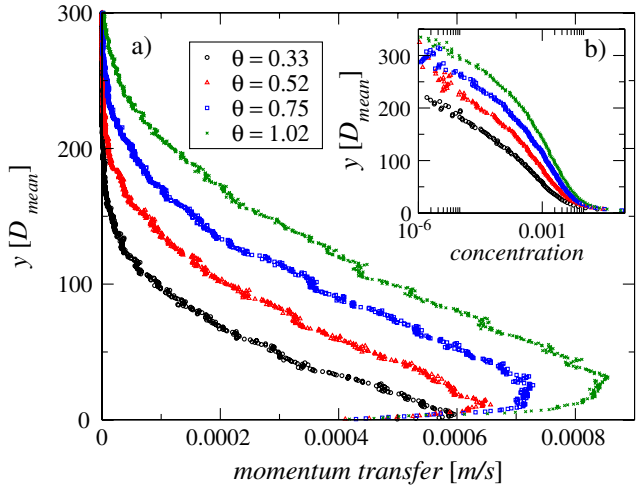

FIG. 4 (color online). Momentum exchange in y direction becomes nonmonotonic as function of height as we increase the Shield number. In the bottom part, it increases with the wind velocity due to the high concentration of particles. The concentration shown in the inset decays logarithmically for lower velocities but has a pronounced inflection point for higher velocities.

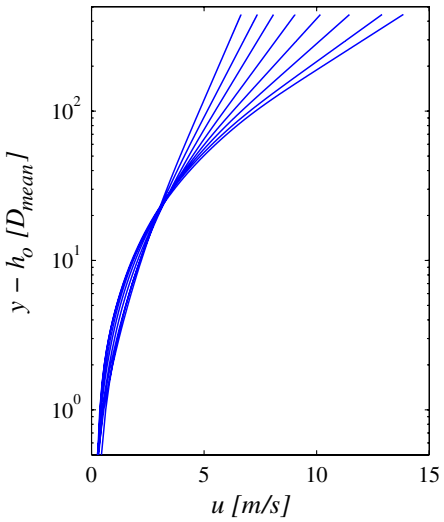

FIG. 5 (color online). Modified wind profiles intersect for $\theta > \theta_c$ at the Bagnold focus. This estimate corroborates measurements for a particle size $D_{\text{mean}} = 200\ \mu$m [7,18,19,31].

sand bed, which is in qualitative agreement with measurements and theory [7,18,19,31].

In summary, we performed particle simulations without any assumption concerning particle trajectories or splash and revealed that the transition is discontinuous with a metastable state for aeolian saltation never reported before. In the metastable region, perturbations or lift forces are required to keep saltation going. It would be interesting to reanalyze or remake experiments of saltation very close to the onset to verify the predicted jump. The existence of a discontinuity at the threshold of turbulent particle transport can have far-reaching consequences in numerous applications ranging from dune mitigation or pneumatic transport to the understanding of Martian landscapes.

This work has been supported by the National Council for Scientific and Technological Development CNPq, Brazil, and ETH Grant (No. ETH-10 09-2). Authors also acknowledge discussions with Dirk Kadau, Allen Hunt, and Klaus Kroy.

[1] R. Greeley and J. D. Iversen, *Wind as a Geological Process on Earth, Mars, Venus and Titan* (Cambridge University Press, New York, 1985).
[2] Y. Shao, *Physics and Modelling of Wind Erosion* (Kluwer Acadademic, Dordrecht, 2008).
[3] R. A. Bagnold, Proc. R. Soc. A **157**, 594 (1936).
[4] R. A. Bagnold, Geograph. J. **89**, 409 (1937).
[5] R. A. Bagnold, *The Physics of Blown Sand and Desert Dunes* (Methuen, New York, 1941), p. 265.
[6] R. Greeley *et al.*, Sedimentology **43**, 41 (1996).
[7] J. E. Ungar and P. Haff, Sedimentology **34**, 289 (1987).
[8] R. S. Anderson and P. K. Haff, Science **241**, 820 (1988).
[9] R. S. Anderson and P. K. Haff, *Mechanics*, Aeolian Grain Transport (Springer, New York, 1991), p. 21.
[10] F. Rioual, A. Valance, and D. Bideau, Phys. Rev. E **62**, 2450 (2000).
[11] F. Rioual, Ph.D. thesis, University of Rennes 1, 2002.
[12] F. Rioual, A. Valance, and D. Bideau, Europhys. Lett. **61**, 194 (2003).
[13] L. Oger, M. Ammi, A. Valance, and D. Beladjine, Comput. Math. Appl. **55**, 132 (2008).
[14] G. Sauermann, K. Kroy, and H. J. Herrmann, Phys. Rev. E **64**, 031305 (2001).
[15] E. J. R. Parteli and H. J.Herrmann, Phys. Rev. Lett. **98**, 198001 (2007).
[16] M. P. Almeida, J. S. Andrade, and H. Herrmann, Phys. Rev. Lett. **96**, 018001 (2006).
[17] M. P. Almeida, E. J. R. Parteli, J. S. Andrade, and H. J. Herrmann, Proc. Natl. Acad. Sci. U.S.A. **105**, 6222 (2008).
[18] J. F. Kok and N. O. Renno, J. Geophys. Res. **114**, 149 (2009).
[19] B. Andreotti, J. Fluid Mech. **510**, 47 (2004).
[20] J. T. Jenkins, I. Cantat, and A. Valance, Phys. Rev. E **82**, 020301(R) (2010).
[21] I. K. McEwan and B. B. Willetts, J. Fluid Mech. **252**, 99 (1993).
[22] J. Nikuradse, *Strömungsgesetze in Rauhen Rohren*, in Forschungsheft 361, Teil B, Vol. 4 (VDI Verlag, Berlin, 1933).
[23] G. H. Keulegan, J. Res. Natl. Bur. Stand. **21**, 707 (1938).
[24] N. S. Cheng, J. Hydraul. Eng. **123**, 149 (1997).
[25] See Supplemental Material at http://link.aps.org/supplemental/10.1103/PhysRevLett.107.098001 for further details about the calculation of the wind profile and interparticle collisions.
[26] W. S. Chepil, Trans., Am. Geophys. Union **39**, 397 (1958).
[27] M. Griebel, S. Knapek, and G. Zumbusch, *Numerical Simulation in Molecular Dynamics: Numerics, Algorithms, Parallelization, Applications* (Springer, New York, 2007).
[28] J. D. Iversen and K. R. Rasmussen, Sedimentology **46**, 723 (1999).
[29] K. Lettau and H. Lettau, *Exploring the World's Driest Climate*, edited by K. Lettau and H. Lettau (University of Wisconsin Press, Madison, 1977).
[30] F. Durst, D. Milojevic, B. S. Eulerian, and Lagrangian, Appl. Math. Model. **8**, 101 (1984).
[31] B. T. Werner, Ph.D. thesis Caltec, Pasadena , 1987.